Lineament Analysis of Landsat Thematic Mapper Images, Northern Territory, Australia

A. Mah, G.R. Taylor, P. Lennox, and L. Balia

Abstract

Lineament analysis of the edge-enhanced Palm Valley Landsat TM images has defined major E-W, N-S, and a NNW-SSE, NNE-SSW conjugate set of lineaments. Two stages of deformation are proposed to have resulted in the development of the Palm Valley arcuate anticline. The stage-one deformation, with the maximum principal stress σ1 oriented in the N-S direction, generated the major gently plunging, E-W trending anticline. The stage-two deformation, with the maximum principal stress σ1 oriented in the E-W direction, was responsible for transforming the gently plunging, E-W trending anticline into an arcuate anticline. The western limb was rotated from E-W trending to WSW-ENE and the eastern limb from E-W trending to NW-SE trending. The first-stage shear fractures on the convex side of the arcuate anticline were transformed into extension fractures in this second stage. The surface and drill logging fractures study of do Rozario and Baird (1987) indicates that surface and subsurface fractures are related. Hence, the fracture system of the Palm Valley arcuate anticline can aid subsurface gas exploration in the area.

Introduction

The Palm Valley Gas Field is located in the Central Northern Amadeus Basin, Northern Territory, Australia (Figure 1) and is operated by Magellan Petroleum (N.T.) Pty. Ltd. on behalf of the Palm Valley Joint Venture. Gas is trapped mainly in fractures within subsurface Ordovician rocks (Milne and Barr, 1990). To date, seven holes have been drilled, and gas reserves have been estimated to be 680 billion standard cubic feet of proven recoverable gas (Milne and Barr, 1990).

The lineament analysis described in this paper is an attempt to better constrain the geological structure and to improve the understanding of the developments of the Palm Valley arcuate anticline and its fractures, lineaments, and faults. These structures are important for gas exploration in this area.

Geology of the Area

The geology of the Palm Valley area has been previously studied by Wells *et al.* (1970), Jackson *et al.* (1984), do Rozario and Baird (1987), Bradshaw and Evans (1988), Mah (1989), and Milne and Barr (1990). The stratigraphy of the Amadeus Basin consists of three main groups of Paleozoic sediments: the Pertnjara, Larapinta, and Pertaoorrta Groups, and minor sediments of Late Proterozoic age (Figure 2) (do Rozario and Baird, 1987).

Surface outcrop in the Palm Valley area is mainly of Late Devonian Hermannsburg Sandstone; a sequence of red-brown sandstones with minor conglomerate and conglomeratic sandstone (Wells *et al.*, 1970; Mah, 1989). Gas is trapped in fractured Ordovician sediments of the subsurface Stairway Sandstone, Horn Valley Siltstone, and Pacoota Sandstone (Figure 2).

The Hermannsburg Sandstone forming the Palm Valley ranges crops out in an approximately east-west trending, gently dipping, arcuate anticline (do Rozario and Baird, 1987). The western and eastern plunges are poorly defined; however, its axis can be traced for over 40 kms. The tectonic history of the area is complex, and deformation occurred during the Late Devonian to Early Carboniferous Alice Springs Orogeny (Jackson *et al.*, 1984; do Rozario and Baird, 1987).

Lineament Analysis of Palm Valley Landsat TM Images

This study used Landsat Thematic Mapper images of Palm Valley which were acquired on 26 August 1986. The study area sub-scene comprises 530 lines by 1024 pixels and is centered on 24°01'42"S by 132°43'E.

Image Enhancement Technique

To highlight the lineaments, TM bands 4, 5, and 7 of the Palm Valley area were edge-enhanced by 3 by 3 asymmetric filter kernels with different illumination directions. TM 7 was filtered with a NE-SW trending illuminated filter; TM 5 was filtered with a NW-SE trending illuminated filter, and TM 4 was filtered with E-W and N-S trending illuminated filters. The filtered images are shown in Plate 1. The filtered TM 7 image (Plate 1a) highlighted all the NW-SE trending lineaments and those in their vicinity; for example, NNW-SSE and WNW-ESE trending lineaments were also highlighted because the illumination direction was from the NE-SW. Similarly, the NW-SE filtered TM 5 (Plate 1b) highlighted the NE-SW, NNE-SSW, and ENE-WSW trending lineaments. N-S and E-W filtered TM 4 (Plates 1c and 1d) highlighted E-W, ENE-WSW, ESE-WNW, and N-S, NNW-SSE, and NNE-SSW trending lineaments, respectively. A color composite of N-S filtered TM 4 (blue), NW-SE filtered TM 5 (green), and NE-SW filtered TM 7 (red) was constructed (Plate 1e). All the filtered images and the color composite show the filtered lineaments well, but the topography is not well defined. To retain the general topography of the area and at the same time highlight the lineaments, edge-enhanced images are added back to the original bands using the following formula and then combined to form a color composite (Plate 1f):

Department of Applied Geology, University of New South Wales, P.O. Box 1, Kensington, NSW 2033, Australia.

Photogrammetric Engineering & Remote Sensing, Vol. 61, No. 6, June 1995, pp. 761–773.

0099-1112/95/6105–761$3.00/0

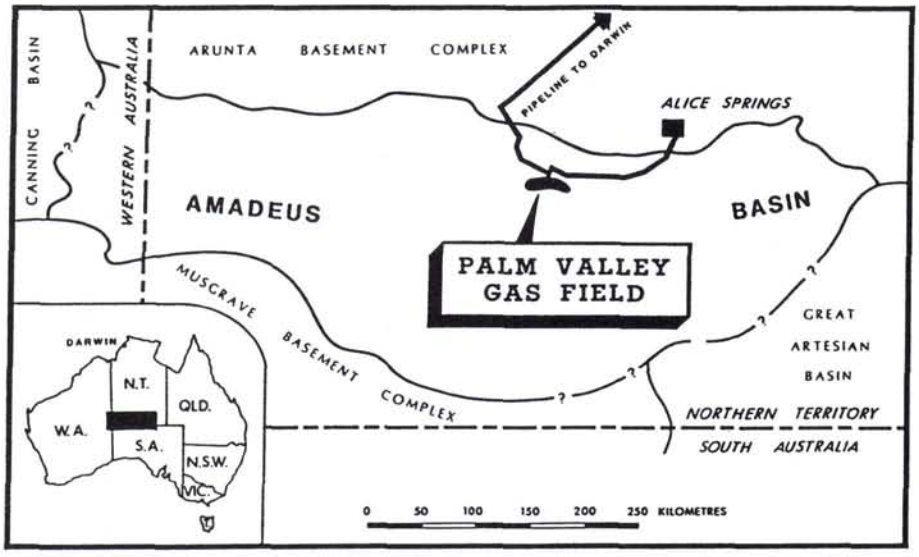

Figure 1. Location map of Palm Valley Gas Field (modified after do Rozario and Baird, 1987).

TM 7 (blue) = NE-SW filtered data 20% + original data 80%
TM 5 (green) = NW-SE filtered data 20% + original data 80%
TM 4 (red) = E-W filtered data 15% + N-S filtered data 15% + original data 70%

Lineaments are used to describe linear topographic features of regional extent that are believed to reflect crustal structure (Hills, 1972). In the present study, lineaments in the relevant area are believed to be due to erosion along fractures, either faults or sets of joints. Because small scale fractures and joints reflect regional structures (Hancock, 1985), lineaments as short as 100 m are interpreted from the TM images. Fractures are defined in the *Glossary of Geology* (Gary *et al.*, 1973) as a general term for any break in a rock, whether or not it causes displacement due to mechanical failure by stress. Fractures include cracks, joints, and faults (Gary *et al.*, 1973).

One-thousand eighteen lineaments that are straight, parallel, or subparallel (less than 30° azimuth) that are adjacent to each other (Wise, 1982) and are longer than 100 m are manually interpreted as lineaments from the edge-enhanced color composite. Subsurface fractures from drill hole loggings and surface fractures have been studied and compared, and they generally show similar trends (do Rozario and Baird, 1987). Thus, understanding the surface structure and fractures and their development will provide an insight into the subsurface structure. Open fractures in the Pacoota Sandstone, Horn Valley Siltstone, and Stairway Sandstone will be important as a fracture reservoir for gas.

Lineament Interpretation from the TM Imagery

The interpreted lineaments were statistically analyzed using the LINPAC software developed by Balia and Taylor in 1990 at the University of New South Wales, Sydney, Australia. Both the azimuth frequency and total length rose diagrams and their respective histograms (Figures 4a, 4b, 4c, and 4d) indicate that there are two major groups of lineaments in the studied area. These groups comprise lineaments trending between 330° to 020° (Figure 5) and 070° to 110° (Figure 6).

Lineaments between azimuths 330° and 020° comprise prominent N-S and an acute angle conjugate set (NNW-SSE and NNE-SSW) (Figure 5). The NNW-SSE and NNE-SSW acute angle conjugate set of lineaments are particularly concentrated in the central part of the area (Figure 5). Another distinct set of lineaments striking NNW-SSE are concentrated in the eastern part of the area.

The second major group of lineaments (070° to 110°) includes abundant E-W trending lineaments that are concentrated along the 2010000 northing line in the central part of the area (Figure 6). Two other sets of lineament within this second major group occur within distinct geographical areas. One set strikes between 070° and 080° and occurs mainly in the central western part of the study area, and the other set has a trend between 100° and 110° and occurs in the southeastern and southwestern parts of the area (Figure 6).

Field Fracture Mapping

Fractures were mapped in the field at 347 locations within areas A, B, and C (Figure 7).

Fracture Styles

There are high angle to vertical fractures and low angle fractures (less than 30°) subparallel to the bedding observed throughout the surveyed areas. The low angle fractures were probably caused by shearing along the bedding planes of the Hermannsburg Sandstone during flexural-slip folding as the Palm Valley anticline developed (Rowland, 1986; Tanner, 1989). The subsurface Pacoota Sandstone is overlain by 6000 m of younger sediments. The high lithostatic load would have caused the existing low angle fractures that were parallel to subparallel to bedding planes to be closed, and it is therefore unlikely that the low angle fractures along bedding planes will be a significant source of permeability for gas or oil movement.

Orthogonal fractures forming **T**- and **H**-shaped, non-cross cutting sets (Figures 8a and 8b) indicate two distinct periods

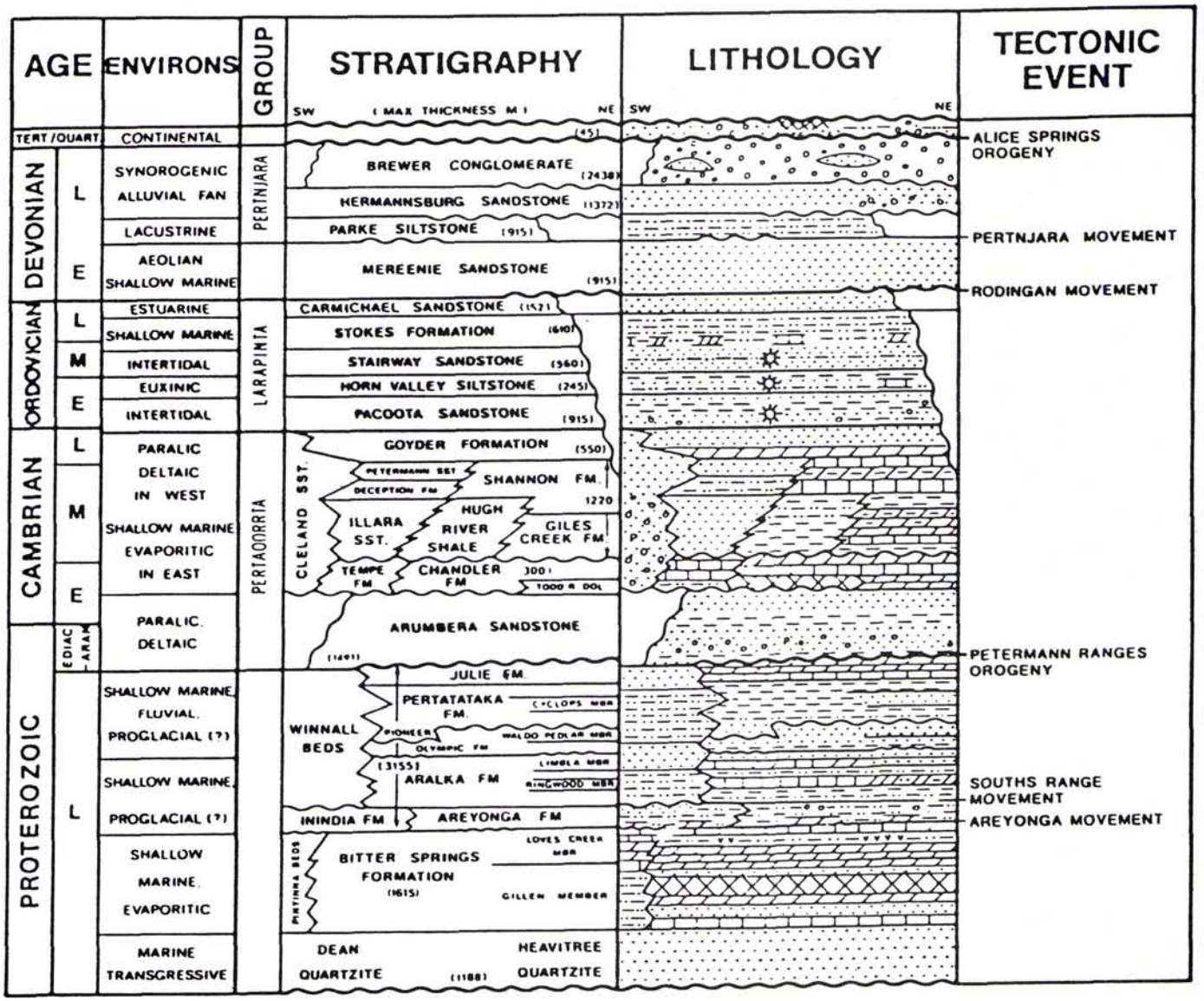

Figure 2. Stratigraphy of the Amadeus Basin (after do Rozario and Baird, 1987).

of systematic extension-fracturing (Hancock, 1985). Conjugate fractures which form **X** and **Y** shapes suggest a hybrid origin and commonly have dihedral angles between 10° and 50°. *En echelon* fractures within the surveyed area indicate a period of shear stress (Figures 8c and 8d).

Fracture Analysis

During anticline formation, fractures at high angle to the bedding are usually formed initially (Stearns, 1968). High angle to vertical fractures encountered in the Palm Valley area are assumed to have developed during arcuate anticline formation. In order to understand the development of the Palm Valley arcuate anticline, high angle to vertical fractures of the area are analyzed. Areas A and B are further divided into subareas A-1, A-2, B-1, and B-2 (Figure 7). The arcuate anticlinal axis forms the dividing line for these subareas. Directional rose diagrams of the subdivided areas and area C drawn using 10° intervals are illustrated on the base map (Figure 7).

The directional rose diagrams indicate the following fracture patterns in the surveyed areas:

- One major E-W (±10°) trending fracture set is encountered in all the surveyed areas;
- One major N-S to N10-20°W trending fracture set is prominent in areas A-2, B-1, B-2, and C, but is less prominent in area A-1; and
- A NE-SW trending fracture set is well developed in area A-2, but is less well developed in area A-1.

Comparison between Fractures Observed in the Field and the Lineament Interpreted from the TM Color Composite Image

The lineament analysis on edge-enhanced Palm Valley TM images is on a regional scale, whereas the field fracture study

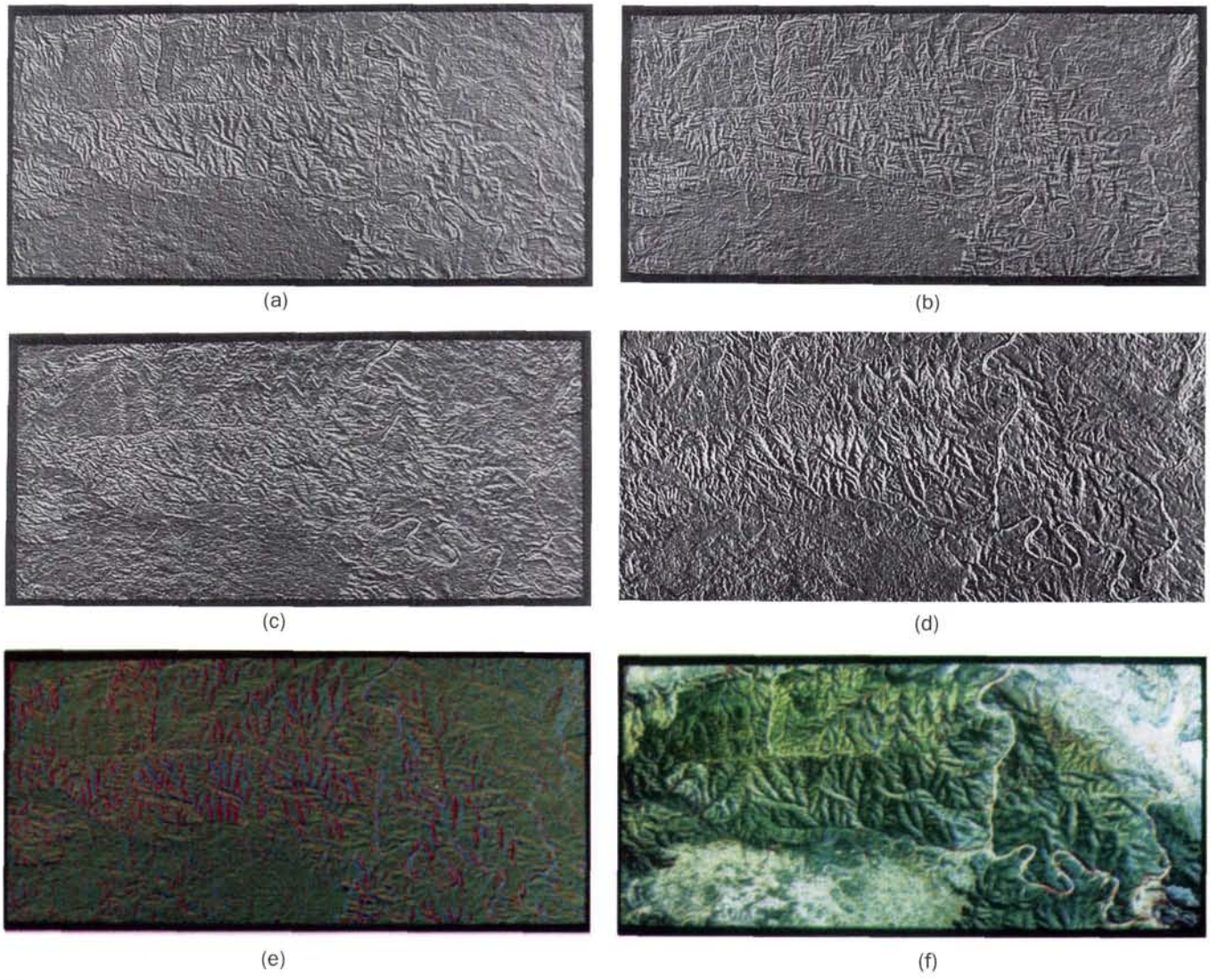

Plate 1. (a) NE filtered TM7 image. (b) NW filtered TM5 image. (c) E-W filtered TM4 image. (d) N-S filtered TM4 image. (e) Color composite of NE filtered TM7 (red), NW filtered TM5 (green), and N-S filtered TM4 (blue). (f) Color composite of edge-enhanced TM4 (red), TM5 (green), and TM7 (blue) with original bands added back to respective filtered images.

is on a local scale. The number of measurements made in the field and the lineaments (also with 10° azimuth interval) interpreted from the TM images in the same field areas are compared in Table 1.

If we assume that the measured field fractures in the studied areas are representative of broader areas of the TM images as defined in Figure 9, comparison of the two data sets is valid (Figures 7, 9, and 10).

Comparison between the field fractures and the lineaments interpreted from TM images of representative blocks are shown in Table 2.

Major E-W, N-S, NNE-SSW, and NNW-SSE fractures and lineaments are comparable between the two techniques. The main fracture directions identified in the field but not recognized as lineaments on the TM images are those that strike ENE-WSW and NE-SW in areas A-1 and A-2, respectively. This may due to the localized existence of field fractures that have not been opened and eroded and hence do not a make deep enough impression on the topography to allow detection using TM images. On the whole, except for ENE-WSW and NE-SW lineaments in areas A-1 and A-2, respectively, the trends of field fractures are in good agreement with the lineaments interpreted from the edge-enhanced Palm Valley TM images.

Discussion

Comparison between Lineament Interpretation from Edge-Enhanced TM Images and Previous Lineament Interpretation from Aerial Photography

Do Rozario and Baird (1987) analyzed the structure of the Palm Valley Ranges using lineaments from conventional photography (Figures 11 and 12).

More lineaments have been interpreted from our edge-enhanced TM images than were interpreted from the aerial photographs (Figures 3 and 11). Do Rozario and Baird (1987)

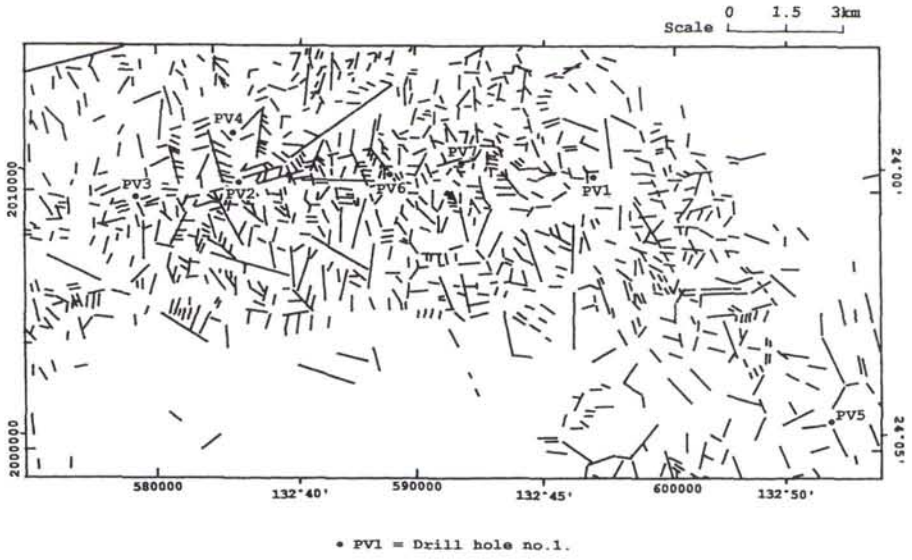

Figure 3. Lineaments of Palm Valley.

identified two major lineament trends: a NW to NNW trend and a NE to ENE trend (Figure 12).

The NNW-SSE and the ENE-WSW trending lineaments of do Rozario and Baird (1987) are equivalent to two sets analyzed from the edge-enhanced TM images. In addition to these sets identified by do Rosario and Baird (1987), the color composite of edge-enhanced TM images additionally show major N-S, E-W, NNW-SSE, and NNE-SSW trending lineament sets.

Model

Do Rozario and Baird (1987) suggested that the Alice Springs Orogeny affected the Amadeus Basin from the Late Devonian to Early Carboniferous, whereas Bradshaw and Evans (1988) extended the deformation due to the Alice Springs Orogeny to Early Permian. Brown *et al.* (1969) suggested that there was no deformation in the Amadeus Basin in the Permian or later. The Late Devonian Hermannsburg Sandstone was affected by the Alice Springs Orogeny during formation of the Palm Valley arcuate anticline with contemporaneous fractures development. The lineaments reflect weathering along these fractures.

Based on all the information acquired from the lineament analysis of the edge-enhanced Palm Valley TM images, the field fracture study, and the spectral analysis of Palm Valley TM images (Mah, 1989), a tectonic model for the evolution of the region has been developed.

It is possible to explain the development of the gently east and west plunging, E-W trending anticline using a one-stage deformation model with $\sigma 1$ in the N-S direction. However, the rotation of the eastern and western limbs towards the south, especially the eastern limb towards the NW-SE, suggests a change in the dominant stress field inconsistent with a continuing maximum compressive stress oriented in the N-S direction. Moreover, the fracture interrelationships observed in the field suggest that the Hermannsburg Sandstone was probably subjected to more than one stage of deformation during the long period of the Alice Springs Orogeny. Where one lineament terminates against another, it can be assumed that the terminated lineament was developed later than the lineament against which it terminates (Hancock, 1985). Among the lineaments interpreted from the edge-enhanced Palm Valley TM images, there are lineaments terminating against lineaments of different orientations, indicating that the lineaments of the Palm Valley arcuate anticline evolved from more than one stage of development (Figure 3). This is also confirmed in the field on small scale fractures where fractures/joints are observed terminating against fractures/joints of different orientations (Figures 8a and 8b). Thus, the development of the Palm Valley arcuate anticline and its structure and lineaments were very likely to

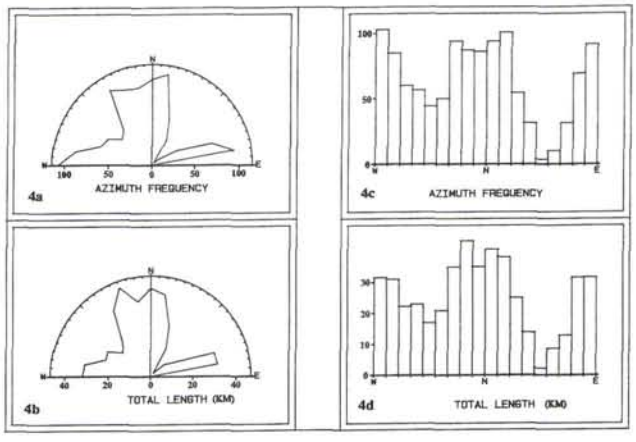

Figure 4. (a) Density (azimuth frequency) directional rose diagram of Palm Valley Lineaments. (b) Length directional rose diagram of Palm Valley Lineaments. (c) Density (azimuth frequency) histogram of Palm Valley Lineaments. (d) Length histogram of Palm Valley Lineaments.

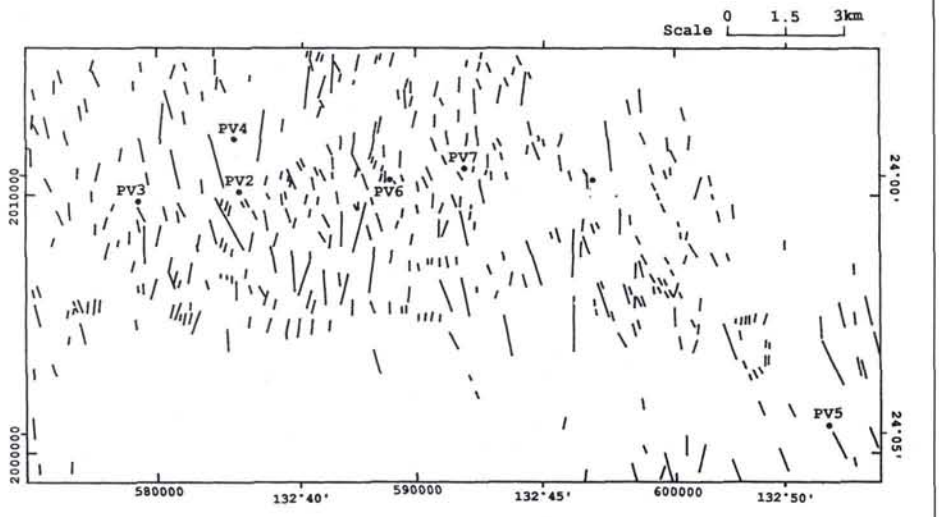

Figure 5. Lineaments of 330° to 020° azimuths.

have developed from more than one stage of deformation. Therefore, they are explained using a model having two stages of deformation.

Stage-One Deformation

This model assumes that, prior to deformation, the Hermannsburg Sandstone was a flat-lying bed (Figure 13).

In the first stage of deformation, a triaxial stress state $\sigma 1 > \sigma 2 > \sigma 3$ affects the sandstone bed, with the first principal compressive stress ($\sigma 1$) from the N-S direction and the third principal stress ($\sigma 3$) from the E-W direction. This formed an E-W trending, doubly plunging anticline with gently dipping limbs (Figure 14). During this deformation, N-S trending extension-fractures (T1) and two sets of conjugate shear fractures (S1, S2) would be generated (Figures 14 and 15a) (Stearns and Friedman, 1972). As the gently dipping and plunging anticline was formed, E-W trending extension fractures (T2) would develop and would be concentrated along the hinge zone of this fold because of extension in this zone (Norman, 1976). Some scattered E-W trending extension fractures would also be found at the northern and southern flanks of the anticline. Especially along the hinge zone and

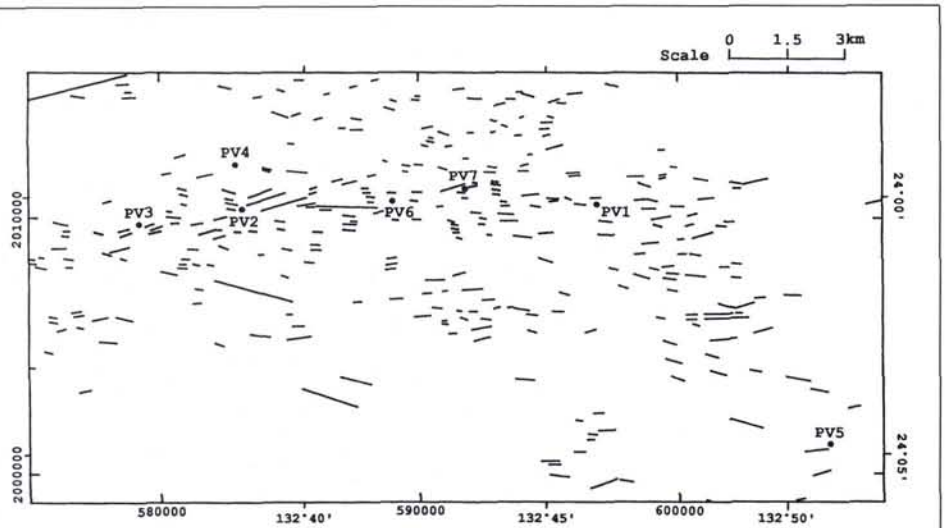

Figure 6. Lineaments of 070° to 110° azimuths.

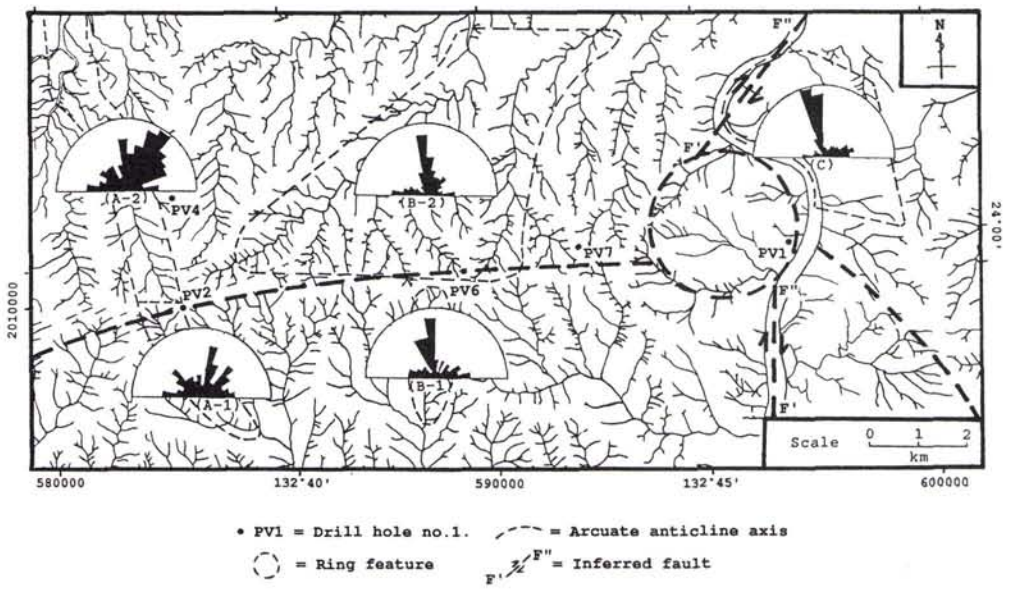

Figure 7. Fractures directional rose diagrams of areas (A-1), (A-2), (B-1), (B-2), and (C) projected on the base map.

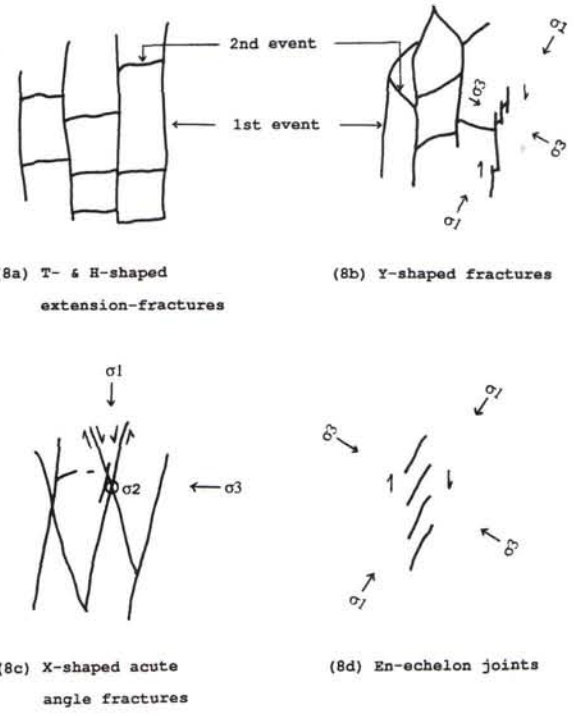

Figure 8. Sketches of the different plan forms of fractures observed in the study area and the likely stress field during their development.

TABLE 1. COMPARISON BETWEEN NUMBER OF FRACTURE MEASUREMENTS MADE IN THE FIELD AND LINEAMENTS INTERPRETED FROM THE TM IMAGES IN THE SAME FIELD AREAS.

Area	Fractures measured in the field	Number of lineaments on TM images in the same field area	Number of lineaments on TM images in representative block (Figure 9)
A-1	110	17	127
A-2	236	25	74
B-1	112	13	97
B-2	824	106	198
C	300	25	52

its vicinity, T1 and T2 are found to be cross-cutting each other or terminating against each other (Figure 3). This relationship suggests that they were formed contemporaneously. S1 and S2 conjugate shear fractures also terminate against each other in different parts of the TM image and also with T1 and T2. This suggests that these fractures were also formed contemporaneously. Shear fractures along the bedding and cross-bedding planes (S3) would develop during flexural-slip folding in which the upper bed slipped over the lower bed to accommodate the buckling (Tanner, 1989). At the initial stage of the formation of the open fold, the local stress field on the flanks of the open fold would be responsible for S11 (ESE-WNW) and S22 (ENE-WSW) conjugate shear fractures (Stearns, 1968) (Figure 14). T1, T2, S1, and S2 are seen terminating against S11 and S22, indicating that S11 and S22 are the earliest lineaments formed during this first stage of deformation.

Stage-Two Deformation

In the second stage, the first principal stress σ1 would be oriented in an E-W direction (Figure 16). This second-stage de-

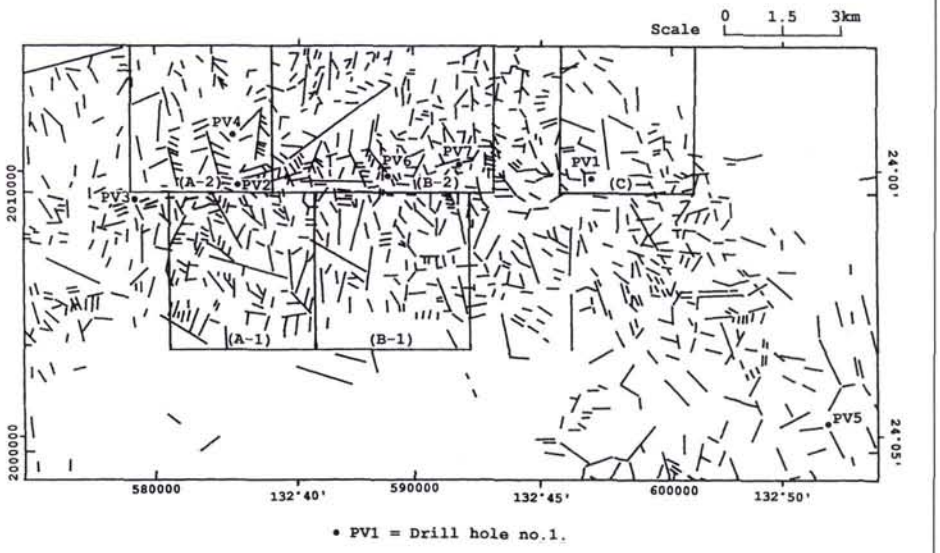

Figure 9. Lineaments of Palm Valley with representative blocks of areas (A-1), (A-2), (B-1), (B-2), and (C).

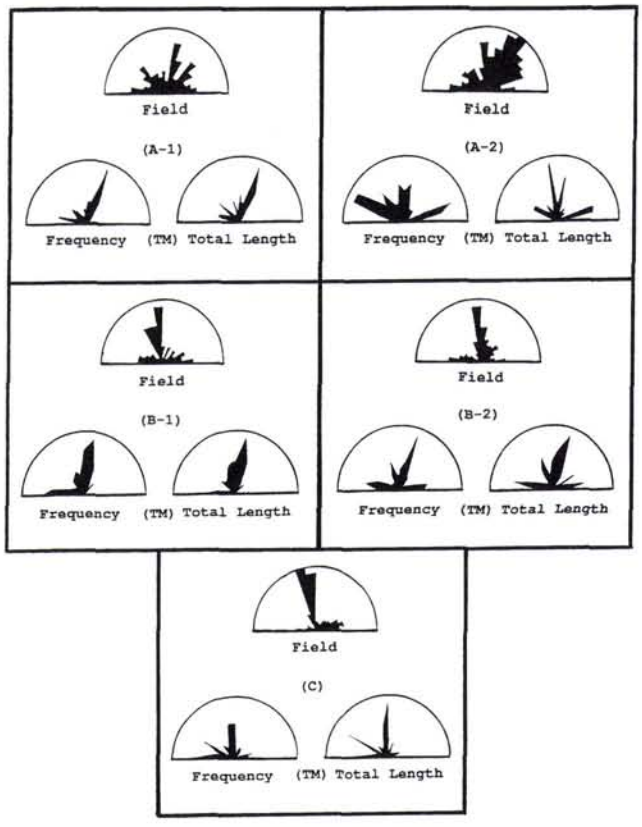

Figure 10. Comparison between rose diagrams of field fracture data from areas (A-1), (A-2), (B-1), (B-2), and (C) with rose diagrams (frequency and total length) of lineaments interpreted from representative blocks of the respective areas on edge-enhanced TM images.

formation was responsible for the sinistral and dextral drags that rotated the western and eastern limbs, respectively, of the anticline to the south.

TABLE 2. COMPARISON BETWEEN FIELD FRACTURES AND LINEAMENTS INTERPRETED FROM TM IMAGES OF REPRESENTATIVE BLOCKS.

Area	Field	TM images (Frequency Rose diagram)	TM images (Length Rose diagram)
A-1	E-W NNE-SSW NW-SE ENE-WSW	E-W NNE-SSW NW-SE ENE-WSW lineaments are missing	E-W NNE-SSW NW-SE ENE-WSW lineaments are missing
A-2	N-S NW-SE E-W NE-SW	N-S NW-SE E-W (minor) NE-SW lineaments are missing	N-S NW-SE E-W (minor) NE-SW lineaments are missing
B-1	N-S NNW-SSE E-W NNE-SSW (minor)	N-S NNW-SSE E-W NNE-SSW	N-S NNW-SSE E-W NNE-SSW
B-2	E-W N-S NNW-SSE NNE-SSW	E-W N-S (minor) NNW-SSE NNE-SSW	E-W N-S (minor) NNW-SSE NNE-SSW
C	N-S E-W NNW-SSE NW-SE (minor)	N-S E-W NNW-SSE (minor) NW-SE	N-S E-W NNW-SSE (minor) NW-SE

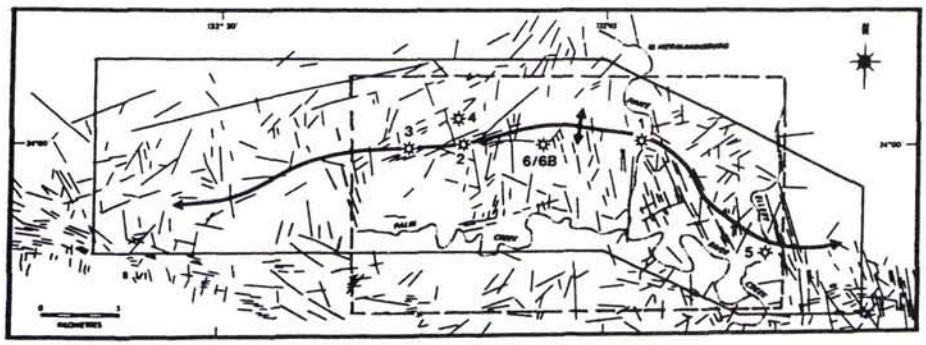

Figure 11. Lineaments of Palm Valley interpreted from aerial photographs and the Palm Valley anticline axis (after do Rozario and Baird, 1987).

Lineaments Development Due to Limb Rotation

During the initial stage of the formation of the arcuate anticline, shear fractures (S6) would be formed. S6 shear fractures developed along the direction of ENE-WSW (070°-080°) in the northwestern part of the area and also developed in the eastern part of the anticline in the direction of 340°-350° (Figures 15b and 16). Compression on the concave side of the arcuate anticline would form conjugate shear fractures S4 (western end) and S5 (eastern end) (Figures 15b and 16). Both are in the orientation of 100° to 110°. Conjugate shear fracture S4 was more developed in the western part and S5 was more developed in the eastern part of the concave side of the arcuate anticline. It is common in folds for one of the conjugate shear fractures to be better developed compared with the other. Though S4 and S5 are of the same orientation (110°-110°), they are not the same fracture set. In the western part of the concave side, S4 is oriented at an obtuse angle to S6 whereas, in the eastern part of the concave side, S5 is oriented at an acute angle to S6. S5 and S6 terminate against each other on the eastern part of concave side, indicating that both were formed more or less contemporaneously (Figure 3). On the western concave side of the arcuate anticline, S6 was not well developed. The nature of its cross-cutting relationship with S4 is not clear. S6 lineaments, especially in the northwestern part of the area, are seen terminating against T1 and S2 of stage-one lineaments. S4 and S5 are terminating against stage-one lineaments such as T2 and S2 on the concave side of the arcuate anticline. All these indicate that S4, S5, and S6 lineaments are formed during the second-stage deformation.

Seismic studies of the area indicate that a diapir involving salt in the Bitter Springs formation beneath the Pacoota Sandstone (Bradshaw and Evans, 1988) has caused the ring feature (T5) observed in the central eastern part of the area (Figure 16) (Mah, 1989). The bulging of the salt in the Bitter Springs formation created extensional radial and ring fractures which are seen on the TM images as the ring feature. E-

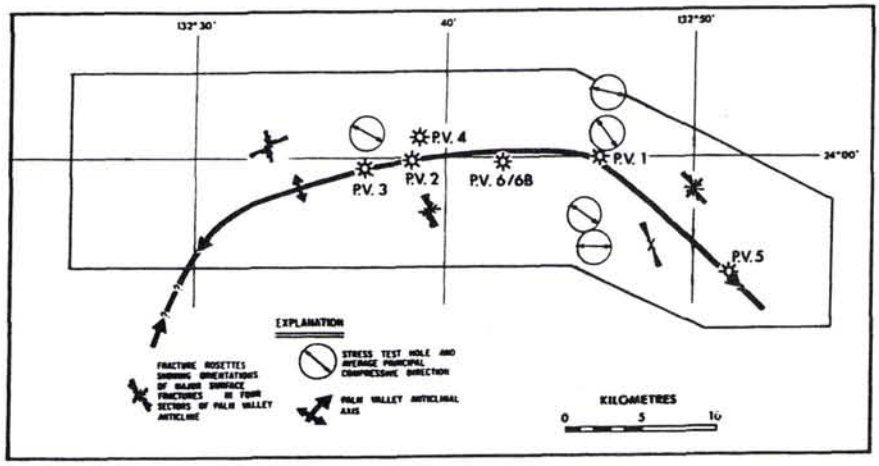

Figure 12. Directional rose diagram of lineaments of four local areas interpreted from aerial photographs and the Palm Valley anticlinal axis (after do Rozario and Baird, 1987).

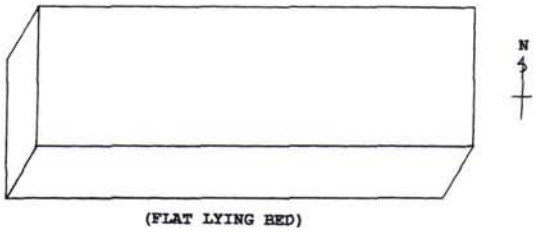

Figure 13. Initial stage.

W extension fractures (T2) and some extension fractures of T1, T3, and T4 have cut through the northern part of the ring feature which lies mainly on the fold axis trace of the anticline. This relationship suggests that salt intrusion, arcuate anticline development, and fracturing occurred contemporaneously.

Lineaments Reactivated During the Second Stage of Deformation

The second-stage deformation, with the first principal stress $\sigma 1$ in the E-W direction, converted the shear fractures S1 and S2 into extension fractures T3 and T4 on the convex side of the arcuate anticline, and changed all the N-S extension fractures (T1) and the two sets of shear fractures (S1, S2) on the concave side of the arcuate anticline formed during the stage-one deformation into compression fractures C1, C2, and C3, respectively (Figures 15b and 16).

Shear fractures S22 of the first stage are assumed to have acted as extension fractures (T22) during extension of the convex side of the arcuate anticline (Figures 3, 14, and 16). T22 extension fractures are parallel to S6 shear fractures of the second-stage deformation, and similarly, S11 shear fractures of the first-stage deformation are parallel to S4 shear fractures of the second-stage deformation. Nevertheless, it is possible to differentiate between T22 and S6 and between S11 and S4, because both T22 (S22) and S11 are prominent (1.5- to 3.2-km-long lineaments), and moreover, as discussed above, S11 and T22 (S22) were the earliest formed lineaments in the stage-one deformation (Figures 3 and 16). S6 and S4, on the other hand, are shorter in length and are terminating against stage-one lineaments such as T1, C2 (S1), and C3 (S2), indicating that they developed during the second stage of deformation (Figure 3). On the eastern limb, S22 shear fractures of the first stage would also have been transformed into extension fractures due to extension on the convex side of the arcuate anticline. It would also be parallel to S6 shear fractures of the second stage. However, on the eastern limb, T22 extension fractures are not prominent and are not well developed. Moreover, there is no evidence of lineaments terminating against S6, which would indicate that these fractures are of the first stage, thus enabling assignment of those lineaments as T22. S11 shear fractures of the first-stage deformation were also not prominent and not well developed in the eastern limb. During the later period of the second-stage deformation, extension of the arcuate anticline would transform the initial second-stage shear fractures S6 into extension fractures (T66) on the convex side of the arcuate anticline (Figure 16).

Contemporaneously, sinistral drag gradually rotated the E-W trending lineaments in the central western region counter-clockwise to a maximum azimuth of 070°, and dextral drag in the central eastern part of the area gradually rotated the E-W trending lineaments clockwise to a maximum azimuth of 135° (Figure 16). The reason for the asymmetrical arcuate anticline is that, during the rotation of the eastern limb to the south, basement faults were reactivated along the weak zones of the Finke River (Bradshaw and Evans, 1988) and the eastern limb was dragged more to the south with the rotation centered on the ring feature (Figures 16 and 17).

If a single-phase model is considered, to develop an arcuate anticline from a E-W trending flat lying Hermannsburg sandstone, $\sigma 1$ could be oriented at approximately N53°E ± 10°. The following features would develop from such a single-phase model:

- The arcuate anticline would have developed with the eastern and western limbs bent towards the south. The western limb may bend slightly towards the south; however, the eastern limb would not rotate towards the NW-SE because it would require a change in the dominant stress field inconsistent with a continuing maximum compressive stress oriented in the N53°E ± 10° direction.
- Prominent extension fractures along the arcuate anticline axis.
- Prominent N53°E ± 10° extension fractures.
- Shear fractures would develop with an E-W ± 10° trending shear fracture dominant on the western limb and prominent N70°W ± 10° trending shear fractures on the eastern limb.

The possible fractures developed by the single-phase model such as E-W ± 10° and N70°W ± 10° trending fractures are observed on the TM images and in the field. The ring structure and inferred faults would also have developed. However, the Palm Valley arcuate anticline with its western limb trending roughly at E-W and the eastern limb trending at almost NW-SE, presence of prominent N-S extension fractures, and lack of prominent N53°E ± 10° fractures both in the

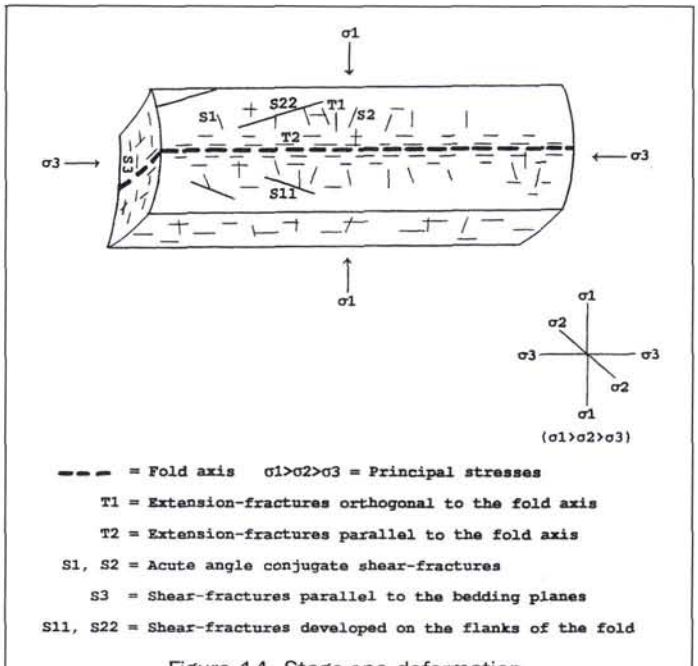

Figure 14. Stage-one deformation.

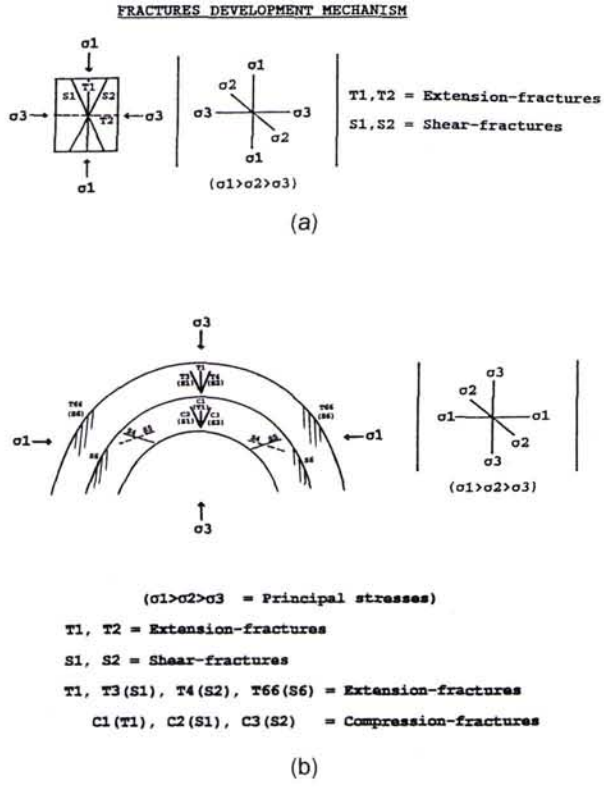

Figure 15. Potential fractures developed during stage one and stage two deformation. (a) Plan view of stage one deformation with σ1 oriented in the N-S direction. (b) E-W oriented cross-section showing stage two deformation with σ1 oriented in the E-W direction.

field (except for area A-2, Figure 7) and on the TM images (Figures 3 and 4) suggest that it is unlikely that the Palm Valley arcuate anticline was developed during a one-phase deformation history.

Because the spatial and temporal development of the lineaments and features observed on the TM images and in the field are consistent with the two-stage model, it is proposed that the two-stage model is more feasible for the development of the Palm Valley arcuate anticline than is a one-stage model.

Conclusion

Lineament analysis of the edge-enhanced Palm Valley TM images has identified major E-W, N-S lineaments and a NNW-SSE, NNE-SSW conjugate set of lineaments and less frequent lineaments trending approximately 070°, 110°, and 340°. Comparison between fractures measured in the field and lineaments interpreted from the edge-enhanced TM images indicates that lineaments are generally parallel to the high angle to vertical fractures measured in the field (Mah, 1989).

A two-stage model of deformation is suggested to explain the history of the observed fracture patterns and the development of the arcuate hydrocarbon-bearing anticline.

The first stage of deformation, with σ1 in a N-S direction, generated the E-W trending anticline, E-W and N-S trending extension fractures, ENE-WSW and ESE-WNW trending conjugate shear fractures, NNW-SSE and NNE-SSW trending conjugate shear fractures, and low-angle to bedding planes (less than 30°) shear fractures.

In the second stage of deformation, σ1 was oriented in an E-W direction. This second-stage deformation was responsible for the development of shear fractures S4, S5, and S6 (Figures 15b and 16). During this second stage of deformation, minor sinistral and major dextral rotation on the western and eastern limbs of the anticline, respectively, occurred while the E-W trending fractures were contemporaneously rotated to trends of 070° and 135° in the central western and central eastern parts of the area, respectively. Localized E-W extension caused opening of the already established N-S trending extension fractures on the convex side of the arcuate anticline and converted the ENE-WSW, NNW-SSE, and NNE-SSW trending shear fractures on the convex side of the arcuate anticline into extension fractures. Compression also converted the N-S trending extension fractures and NNW-SSE and NNE-SSW trending shear fractures on the concave side of the arcuate anticline into compressional shear fractures. The later stage of extension, during the second-stage deformation, also transformed the initial second-stage S6 shear fractures into extension fractures on the convex side of the arcuate anticline.

The result of the lineament analysis suggests that the arcuate anticline of Palm Valley was developed during two stages of deformation in this area. The final stage of deformation resulted in a gentle southwardly rotated limb on the western side but with the eastern limb rotated from a E-W to a NW-SE trend. A ring feature developed in the central eastern part of the area and two major faults developed along the Finke River (Figures 7 and 17).

Folds, faults, and fractures as potential reservoirs are important structural features in oil and gas exploration (Alpay, 1973; Lowell, 1985; do Rozario and Baird, 1987). Because surface and subsurface fractures are directly related (do Rozario and Baird, 1987) and this study has characterized sur-

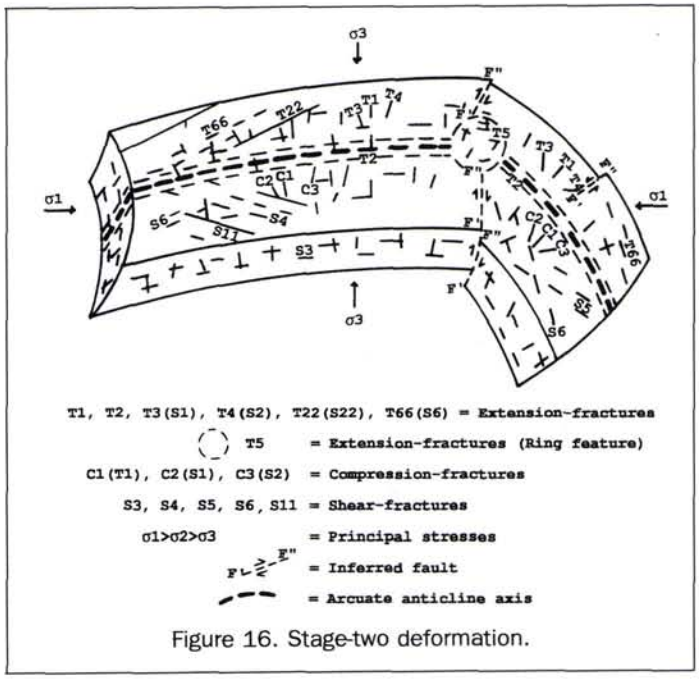

Figure 16. Stage-two deformation.

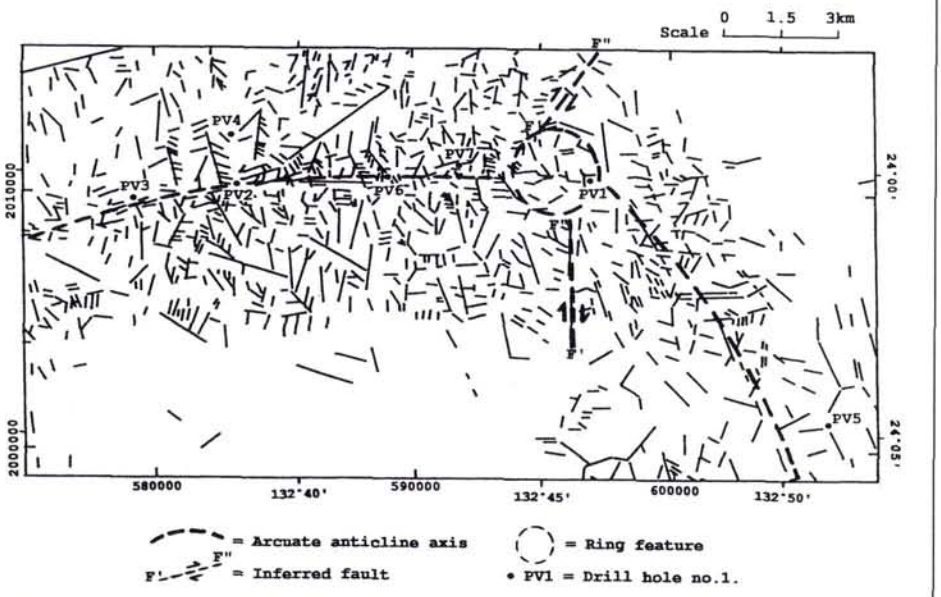

Figure 17. The interpreted Palm Valley Arcuate Anticline with the ring feature and inferred faults.

face fractures, it has an important bearing on our understanding of subsurface fracturing. Hence, the Palm Valley arcuate anticline, the extension fractures on the convex side, the compression fractures and shear fractures on the concave side of the anticline, the ring feature, and the faults running along the Finke River will be important structural features affecting subsurface gas exploration in this area.

Acknowledgments

The authors wish to thank Magellan Petroleum Australia Limited for providing the computer compatible tape (CCT) of the Palm Valley Landsat TM images and the logistic and financial help that A. Mah received during his field trip. The authors also are indebted to the Centre for Remote Sensing staff, University of New South Wales, for their invaluable assistance. The authors would like to thank the anonymous reviewers for their comments.

References

Alpay, O. A., 1973. Application of Aerial Photographic Interpretation to the Study of Reservoir, Natural Fracture Systems, *Journal of Petroleum Technology*, 25:37–45.

Bradshaw, J. D., and P. R. Evans, 1988. Palaeozoic Tectonics, Amadeus Basin, Central Australia, *The APEA Journal*, 28:267–282.

Brown, D. A., K. S. W. Campbell, and K. A. W. Crook, 1969. *The Geological Evolution of Australia and New Zealand*, Pergamon Press, 409 p.

do Rozario, R. F., and B. W. Baird, 1987. The Detection and Significance of Fractures in the Palm Valley Gas Field, *The APEA Journal*, 27:264–280.

Gary, M., R. McAfee, and C. L. Wolf, 1973. *Glossary of Geology*, American Geological Institute, 805 p.

Hancock, P. L., 1985. Brittle Microtectonics: Principles and Practice, *Jour. of Struct. Geol.*, 7:437–457.

Hills, E. S., 1972. *Elements of Structural Geology*, Chapman and Hall Ltd & Science Paperbacks, 502 p.

Jackson, K. S., D. M. McKirdy, and J. A. Deckelman, 1984. Hydrocarbon Generation in the Amadeus Basin, Central Australia, *The APEA Journal*, 24:42–65.

Lowell, J. D., 1985. *Structural Styles in Petroleum Exploration*, OGCI Publications, Oil and Gas Consultants International Inc., Tulsa, 460 p.

Mah, A., 1989. *Spectral and Lineament Analyses of Palm Valley Thematic Mapper Images (Northern Territory, Australia)*, Master of Applied Science Thesis, University of New South Wales, Australia, 145 p.

Milne, N. A., and D. C. Barr, 1990. Subsurface Fracture Analysis, Palm Valley Gas Field, *The APEA Journal*, 30:321–341.

Norman, J. W., 1976. Photogeological Fracture Trace Analysis as a Subsurface Exploration Technique, *Trans. Instn. Min. Metall. (Sect. B: Appl. Earth Sci.)*, 85:B52–B62.

Rowland, S. M., 1986. *Structural Analysis and Synthesis*, Blackwell Scientific Publications, 208 p.

Stearns, D. W., 1968. Certain Aspects of Fracture in Naturally Deformed Rocks, *NSF Advanced Science Seminar in Rock Mechanics for College Teachers of Structural Geology*, pp. 97–115.

Stearns, D. W., and M. Friedman, 1972. Reservoirs in Fractured Rock, *AAPG Memoir 16*, pp. 82–106.

Tanner, P. W. G., 1989. The Flexural-Slip Mechanism, *Jour. of Struct. Geol.*, 11:635–655.

Wells, A. T., D. J. Foreman, L. C. Ranford, and P. J. Cook, 1970. *Geology of the Amadeus Basin, Central Australia*, Bur. Min. Resour. Bull. 100.

Wise, D. U., 1982. Linesmanship and the Practice of Linear Geo-Art, *Geological Society of America Bulletin*, 93:886–888.

(Received 1 June 1992; revised and accepted 7 September 1993; revised 13 December 1993)

Abdullah Mah
Abdullah Mah has a B.Sc. in Geology, an M.Sc. in Economic Geology, an M.App.Sc. in Remote Sensing, and at present is completing a Ph.D. in Radar Remote Sensing in the Department of Applied Geology, University of New South Wales. He has worked as a geologist in Saudi Arabia and as a structural geologist in Australia. His research interests are in radar remote sensing and application of remote sensing techniques in structural, mineral, and petroleum exploration and environmental problems.

Geoffrey R. Taylor
Geoff Taylor has a B.Sc. in Geology (1967), an M.Sc. in Mineral Chemistry (1968), and a Ph.D. in Economic Geology (1977). He has worked as a geochemist, an economic geologist, and at present is an Associate Professor in the Department of Applied Geology, University of New South Wales. His research interests concern the application of remote sensing and data processing in general to exploration and environmental problems. He is a member of the SIR-C Science Team. He is currently Head of the School of Mines at the University of New South Wales.

Paul Lennox
Paul Lennox obtained a B.Sc. (Hons) from the University of Tasmania (1976) and Ph.D. from Monash University (1985) and is currently a Senior Lecturer in the Department of Applied Geology, University of New South Wales. He has been researching structural geology problems in Australia, Indonesia, and Thailand. His current research is on terranes and granite-country rock relationships in moderately deformed Paleozoic sequences.

Lobo Balia
Lobo Balia has a B.Sc. in Geology (1976), an M.Sc. in Geophysics (1982) and has recently submitted a Ph.D. in the development of remote sensing software for geological exploration. He has worked as a geophysicist, a Data Centre Manager at the Department of Mines and Energy, Indonesia and as a consultant to the United Nations. He is currently project manager at the Department of Mines and Energy, Indonesia, in the field of his research interest which is in the software development for geoscientific applications.